5-2012

Properties of Metal-Graphene Contacts

Joachim Knoch
RWTH Aachen University

Zhihong Chen
Birck Nanotechnology Center, Purdue University, zhchen@purdue.edu

Joerg Appenzeller
Birck Nanotechnology Center, Purdue University, appenzeller@purdue.edu

Knoch, Joachim; Chen, Zhihong; and Appenzeller, Joerg, "Properties of Metal-Graphene Contacts" (2012). *Birck and NCN Publications.* Paper 1198.
http://dx.doi.org/10.1109/TNANO.2011.2178611

Properties of Metal–Graphene Contacts

Joachim Knoch, Zhihong Chen, and Joerg Appenzeller

***Abstract*—We present a study on the metal–graphene contact properties. Utilizing a dual-gate field-effect transistor device, an energetic separation between the Fermi level and the Dirac point in the contact areas can be adjusted deliberately by applying an appropriate front-gate voltage that acts only on the channel. This front-gate voltage is compensated by an opposite large-area back-gate voltage, thereby mimicking the metal induced doping effect. A back-gate voltage sweep enables identifying two distinct resistance peaks—a result of the combined impact of the graphene cones in the contact and in the channel region. Comparing our experimental data with simulations allows extracting the coupling strength between metal and graphene and also estimating the magnitude of the metal-induced doping concentration in the case of palladium contacts. In contrast to conventional metal–semiconductor contacts, our simulations predict a decreased on-current for increased coupling strength in graphene field-effect transistors.**

***Index Terms*—Contacts, graphene, graphene field-effect transistor (GFET), metal–graphene coupling.**

I. Introduction

GRAPHENE is currently attracting increasing attention as an alternative material for future nanoelectronics devices due to its excellent electronic transport properties and the fact that it can, in principle, be patterned using standard planar fabrication technologies [1]–[5]. However, to realize high-performance devices, it is very important to form adequate, highly transmissive metal–graphene contacts. The effect of metal–semiconductor contacts on the performance of an electronic device can, in principle, be characterized by the position of the Fermi level with respect to the conduction/valence bands and the coupling strength between metal and semiconductor [6]–[10]. But since the coupling strength impacts the position of the Fermi level, it is difficult to obtain information on both quantities separately.

In a previous publication by Chen and Appenzeller [11], the properties of metal–graphene contacts were studied using dual-gate graphene field-effect transistors (GFETs) with front- and back-gate. It was found that in contrast to conventional metal–semiconductor contacts, the graphene underneath a contact metal can still be influenced by a gate suggesting a moderate metal–graphene coupling. Due to the importance of contact electrodes for electronic devices, it is, therefore, necessary to study the contact properties in much greater depth. Our dual-gate GFET allows adjusting an energetic separation ΔE_f between the Fermi level and the Dirac point in the contacts by applying an appropriate combination of front- and back-gate voltages, thereby realizing a gate induced doping concentration underneath the contacts that mimics the effect of various work-function differences, i.e., various metals in contact to the graphene. Comparing experimental and simulation data provides access to the metal–graphene coupling strength and the effect of a work-function difference on the electrical properties of the contact electrodes. Recently, Xia *et al*. have presented a study on metal–graphene contacts [12] and concluded that the contact properties are determined by rather large variations of the metal–graphene coupling across the contact area. However, the device in [12] utilized only a single back-gate and hence did not allow us to distinguish between the effect of coupling strength and magnitude of ΔE_f on the electrical characteristics. In fact, our experimental and simulation results provide clear evidence that the coupling strength between the metal electrode and graphene is significantly larger than assumed in [12]. Furthermore, having demonstrated the validity of our simulations by comparison with the experimental data, we study the impact of coupling strength on the device properties. Surprisingly, we find that a better coupling can result in a deteriorated device performance.

II. Resistance Versus Gate-Voltage Characteristics

GFETs with a front- and back-gate were fabricated by growing a 300-nm SiO_2 film onto a heavily doped silicon substrate. After exfoliation, a monolayer of graphene is contacted using Ti/Pd/Au (0.5 nm/20 nm/20 nm) electrodes followed by the deposition of a 10-nm Al_2O_3 employing atomic layer deposition. The devices are finalized by the formation of a Ti/Au (1 nm/40 nm) front-gate electrode [11]. Two different types of devices were fabricated, called A and B in the following. Fig. 1 shows a scanning electron micrograph of the devices and a schematic of the transistor cross sections, respectively. Device A exhibits a channel portion that is gated by both the front- and the back-gate (see Section II) as well as two back-gated-only source/drain extensions (see Sections I). On the other hand, device B consists of a channel that is entirely controlled by both gates. The coupling of a metal to a semiconductor yields a metal-modified density-of-states (DOS) in the semiconductor that depends on the coupling strength: if the coupling is small, the DOS is "semiconductor-like," whereas it resembles the metal DOS in the case of strong coupling. Hence, device types A and B can be considered having a similar structure but with a different coupling strength in the graphene adjacent to

Manuscript received August 9, 2011; revised; accepted November 29, 2011. Date of publication December 20, 2011; date of current version May 9, 2012. The review of this paper was arranged by Associate Editor R. Ruoff.

J. Knoch is with the Institute of Semiconductor Electronics, RWTH Aachen University, 52074 Aachen, Germany (e-mail: knoch@iht.rwth-aachen.de).

Z. Chen and J. Appenzeller are with the Department of Electrical and Computer Engineering and Birck Nanotechnology Center, Purdue University, West Lafayette, IN 47907 USA (e-mail: zhchen@purdue.edu; appenzeller@purdue.edu).

Color versions of one or more of the figures in this paper are available online at http://ieeexplore.ieee.org.

Digital Object Identifier 10.1109/TNANO.2011.2178611

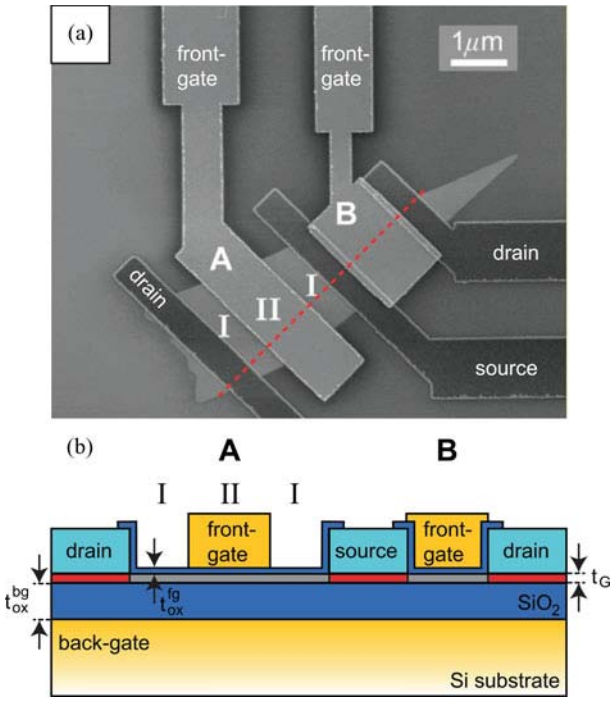

Fig. 1. (a) Electron micrograph of the graphene device structure under investigation. (b) Cross section of the devices of types A and B.

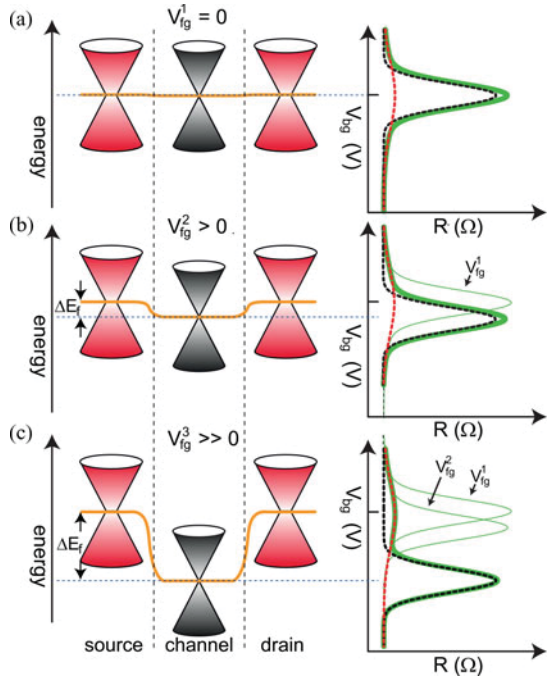

Fig. 2. (a)–(c) Resistance versus back-gate voltage characteristics for different front-gate voltages. The dotted black line represents the main resistance peak, the dotted red line represents the broadened second peak, and the solid green line represents their superposition.

the channel: a vanishing coupling strength in the case of device A in the regions labeled I and a finite coupling in the case of device type B. Applying a constant front-gate voltage $V_{\rm fg}$ results in an energetic separation of the Dirac points in the channel and the contact area. Compensating $V_{\rm fg}$ in the channel by applying an appropriate opposite back-gate voltage $V_{\rm bg}$ leads to a $V_{\rm fg}$-dependent ΔE_f in the contact areas. Two resistance peaks, occurring when either the Dirac point in the channel or the Dirac point in the contacts is aligned with the Fermi level, dominate the resistance R versus $V_{\rm bg}$ characteristics. Since in device type B, separating the Dirac points in the channel and contact areas by applying appropriate $V_{\rm fg}$ and $V_{\rm bg}$ allows investigating the metal–graphene coupling, we will focus on this device type in the following.

Fig. 2(a)–(c) schematically shows R–$V_{\rm bg}$ characteristics together with the respective energetic positions of the cones for three different $V_{\rm fg}$, considering no metal-induced doping in the contact areas (red cones); in (a) and (b) the main resistance peak (dotted black line) associated with the lineup of the Fermi level with the Dirac point of the "gray" cone is superimposed on the second, significantly weaker peak that is a result of the lineup between the metal-modified "Dirac point"of the red cones and the Fermi level. Consequently, only a single peak is observable in these two cases. On the other hand, if ΔE_f is made sufficiently large and the coupling not too strong (which could broaden the second peak such that it becomes unobservable no matter how large ΔE_f is), two resistance peaks appear as shown in Fig. 2(c). At the same time, increasing ΔE_f yields a main resistance peak reduced in magnitude due to a decreasing contribution of the second peak [see Fig. 2(c)]. In the case of strong coupling, the main peak resistance would remain rather unchanged. Hence, a decreasing main peak [see Fig. 3 (a)] with increasing $V_{\rm fg}$ is a clear signature of a resistance contribution of the second peak and thus proves that the coupling between metal and graphene is rather weak although much stronger than had been previously reported [12]. In other words, there are two possibilities that the side peak structure becomes unobservable: 1) a strong coupling with a substantial modification of the DOS in the graphene and 2) an insufficient ΔE_f. With our dual-gate structure, it is possible to adjust ΔE_f and, hence, to study the metal–graphene coupling in greater detail.

Fig. 3(a) displays experimental R–$V_{\rm bg}$ characteristics for several $V_{\rm fg}$. For sufficiently large ΔE_f (i.e., large $V_{\rm fg}$), a second resistance peak can clearly be identified [see the black curve in Fig. 3(a)]. If on the other hand, $V_{\rm fg}$ is too small, the second resistance peak is superimposed by the main resistance peak and thus disappears [see Fig. 3(a)]. Furthermore, the main resistance peak decreases in magnitude for increasing $V_{\rm fg}$ as has been discussed previously. Comparing the experimental data with simulations, we are able to identify the metal–graphene coupling strength. Subsequently, our simulations enable a determination of ΔE_f as a function of $V_{\rm fg}$. In contrast to [12] where it has been argued that a rather large variation of the metal–graphene coupling across the contact prohibits the observability of the second resistance peak, we will argue that in a single-gate GFET, the metal-induced doping is insufficient and that the second peak is not observable due to the superposition of the main resistance peak.

Fig. 3(b) shows R–$V_{\rm fg}$ characteristics for a constant $V_{\rm bg}$. Because a metal in contact with graphene *does not* pin the Fermi level E_f, different gate induced doping concentrations in the

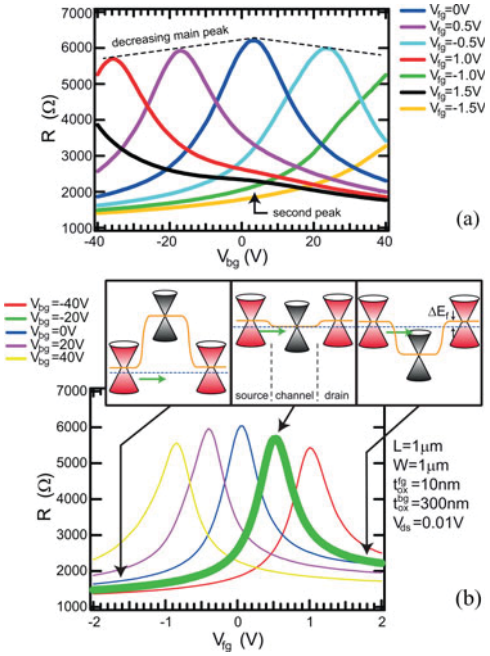

Fig. 3. (a) Resistance versus back-gate voltage for several $V_{\rm fg}$. (b) R versus $V_{\rm fg}$ for different $V_{\rm bg}$. The insets show the respective energetic position of the graphene cones within the contact areas and the channel for the gate voltages indicated by the arrows.

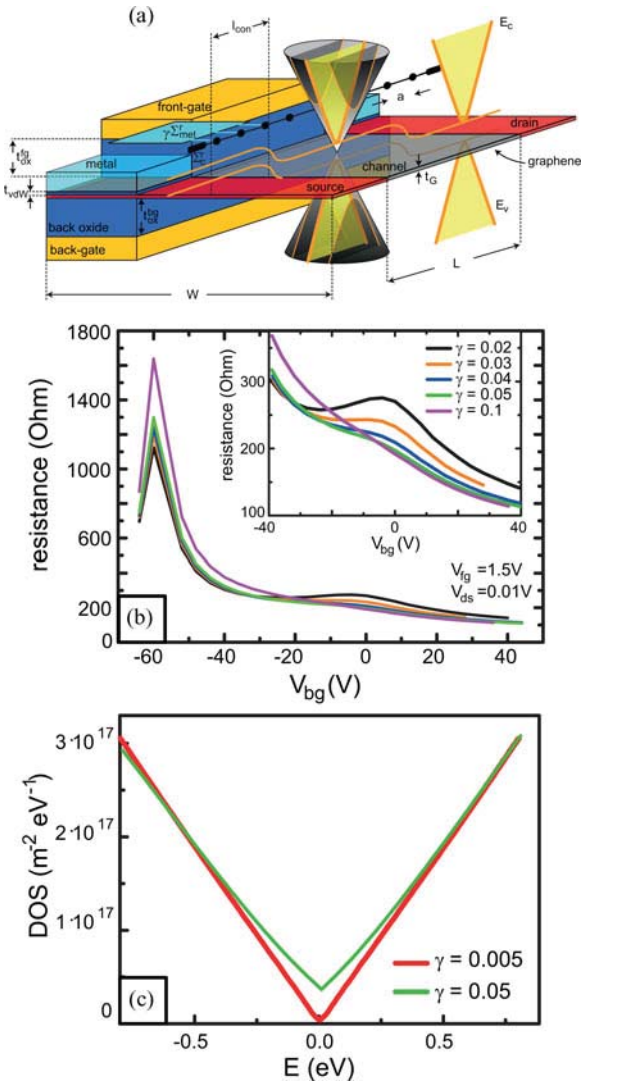

Fig. 4. (a) Simulated device structure. An independent mode-space approach is employed as illustrated by the three intersections between the cone and the planes of constant k-values quantized along the direction of W. (b) Resistance versus back-gate voltage for several coupling strengths. The inset shows the second resistance peak in more detail. (c) Average of the density of states in the contact regions for small and strong coupling conditions.

contacts can be realized by means of $V_{\rm bg}$. Since the front-gate acts only on the channel area, a $V_{\rm fg}$ sweep yields characteristics with a single resistance peak occurring when the Dirac point in the channel is aligned with the source Fermi level. An asymmetric curve for larger or smaller $V_{\rm fg}$ due to Klein tunneling appears [11], [13] as illustrated in the insets of Fig. 3(b) that show the respective energetic positions of the conduction/valence band cones. Furthermore, the larger $V_{\rm bg}$ the smaller is the peak resistance because of a decreased contribution of the red cones to the total resistance. At the same time, the asymmetry becomes more pronounced. Note that a symmetric R–$V_{\rm fg}$ behavior around the main resistance peak belongs to the case where the Dirac points in the contact areas are aligned with the Fermi level by means of an appropriate $V_{\rm bg}$ that compensates the metal-induced doping effect. In the present case, this happens at $V_{\rm bg} \approx 25$ V indicating that the metal electrodes induce a p-type doping.

III. Simulations

In order to investigate the metal–graphene coupling, simulations are performed and compared with the experimental data. Our simulations are based on a self-consistent solution of Poisson's and Schrödinger's equation. For the electrostatics, a surface potential method is employed as appropriate for an ultrathin body transistor such as a GFET [15]. The approach leads to a 1-D modified Poisson equation given by

$$\frac{d^2\Phi_f(x)}{dx^2} - \frac{\Phi_f(x) - \Phi_g}{\lambda^2} = -\frac{e\rho(x)}{\varepsilon_0 \varepsilon_{\rm gra}}. \qquad (1)$$

Here, Φ_g is the gate potential and ρ is the density of mobile carriers. λ is the relevant length scale for potential variations and is a function of the graphene thickness $t_{\rm G}$ as well as the gate oxide thickness $t_{\rm ox}$ reflecting the device geometry under consideration [8], [15]. In the present case, we consider device layout where the back-gate, separated from the graphene by an oxide of thickness $t_{\rm ox}^{\rm bg}$, acts on source, drain, and channel. In source and drain, the metallic electrodes act as additional gates which are a van der Waals distance $t_{\rm vdW}$ away from the graphene. In addition to the back-gate, a front-gate acts on the graphene in the channel area. Fig. 4(a) shows a schematic of the device structure considered here.

The nonequilibrium Green's function formalism on a finite difference grid is used to calculate the charge in and current through the device [14]. An independent mode-space approach

is employed to calculate the 2-D graphene sheet by summing-up the charge and current contributions of appropriate 1-D subbands [see Fig. 4(a)] [16]. In each mode, an energy-dependent effective mass accounts for the linearity of the conduction/valence bands for larger k-values as well as for the complex band structure in the respective bandgap [17], [18]. The metal–graphene contacts are taken into account by attaching Buettiker probes at each node of the finite difference grid within the contact area over a contact length $l_{\rm con}$ [see Fig. 4(a)]. These Buettiker probes share a common Fermi level given by the terminal voltage and are coupled to each subband. The metal–graphene coupling strength is described by a coupling constant $\gamma = 0..1$. Different coupling strengths are a result of a varying metal–graphene separation $t_{\rm vdW}$ or a varying height of the potential barrier in between the metal and the graphene. The present approach has been applied successfully to study the properties of metal–carbon nanotube contacts [6], [8]. In order to keep the computational burden as small as possible, we simulate GFETs with a channel length of $L = 25$ nm, equal front- and back-gate dielectric (SiO_2) thicknesses of $t_{\rm ox} = 3$ nm and a width of the device of $W = 400$ nm resulting in 200 modes that are considered in the simulations.[1] In addition, the thickness of the graphene layer $t_{\rm G}$ and the metal–graphene separation $t_{\rm vdW}$ are both taken to be 3Å; finally, room-temperature conditions and ballistic transport are assumed in all simulations.

Resistance versus $V_{\rm fg}$ and $V_{\rm bg}$ characteristics are simulated and compared with experiments. In order to reproduce the main experimental features, the back-gate voltage dependence was simulated as a function of the metal–graphene coupling strength. In particular, the second resistance peak is of interest since a comparison with the experiments allows estimating the coupling strength γ. Fig. 4(b) shows the resulting curves for several γ; $V_{\rm fg} = 1.5$ V was chosen ensuring that the main and second resistance peaks are clearly distinguishable. Note that the chosen front-gate oxide thickness $t_{\rm ox}^{\rm fg} = 3$ nm results in a similar effective front-gate oxide capacitance as in the experimental case with a 10-nm-thick aluminum oxide. Hence, the simulated curves can be compared with the respective experimental curves for the same front-gate voltage. The back-gate voltage axis, on the other hand, was scaled by a factor of 40 for a proper comparison of simulations with experimental data.[1]

A small coupling leads only to a small modification of the graphene DOS and hence yields a pronounced second resistance peak [see the inset of Fig. 4(b)]. Upon increasing γ, the second resistance peak becomes less pronounced and eventually vanishes completely for $\gamma \geq 0.05$. Fig. 4(c) shows the average local DOS versus energy within the contact regions. In the case of small coupling, the DOS remains almost unmodified. In contrast, the DOS does not vanish anymore at the Dirac point in the case of a stronger coupling.

[1]While the front-gate capacitance is approximately the same in the experiments and simulation, the back-gate oxide thickness in the experiment is significantly larger. Therefore, the back-gate voltages are scaled by a factor of 40 which is approximately the ratio of the voltage differences between main and second resistance peak of experimental [red line in Fig. 3 (a) and simulated curves (which would be 1 V) in the case of a front-gate voltage of 1 V.

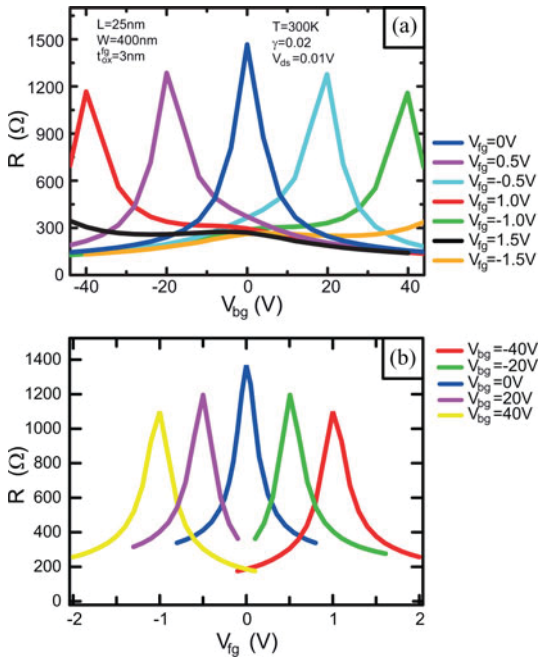

Fig. 5. (a) and (b) Simulated R versus scaled $V_{\rm bg}$ and $V_{\rm fg}$ characteristics with a coupling strength of $\gamma = 0.02$.

Comparing experimental and simulated curves [see Fig. 3(a) and 4(b)], we estimate $\gamma \approx 0.02 - 0.03$. Note that this coupling yields a lifetime broadening of the electronic states on the order of 50–75 meV which is roughly the same as was found by Nemec *et al*. [7]. With $\gamma = 0.02$, we simulated R–$V_{\rm fg}$ characteristics (for different $V_{\rm bg}$) and R–$V_{\rm bg}$ characteristics (for several $V_{\rm fg}$) shown in Fig. 5(a) and (b). Obviously, all experimental features such as the resistance asymmetry, the decreasing peak resistance for increasing $V_{\rm bg}$, and, in particular, the broadened second resistance peak can be reproduced with our simulations [compare with Fig. 3(a) and (b)]; note that the deviation of the absolute resistance values between simulation and experiment is due to scattering in the graphene channel in the experimental case. As a result, we are now in a position to explore the impact of the coupling strength on the characteristics of GFETs in greater detail.

IV. Discussion—Metal–Graphene Contact Properties

We have discussed previously that our dual-gate device structure allows creating different ΔE_f within the contacts mimicking the metal-induced doping effect of various metal–graphene work-function differences. The main panel of Fig. 6(a) shows ΔE_f as a function of $V_{\rm fg}$ extracted from our simulations. The inset shows again the R–$V_{\rm bg}$ characteristics (for the same positive $V_{\rm fg}$ as displayed in the main panel, except $V_{\rm fg} = 2$ V) and $\gamma = 0.02$. Apparently, the resistance peaks can be distinguished clearly only if $V_{\rm fg} \geq 0.75$ V, whereas the observability of the two peaks disappears for smaller $V_{\rm fg}$. The dashed lines in the main panel of Fig. 6(a) show that $V_{\rm fg} = 0.75$ V corresponds to a $\Delta E_f \approx 125$ meV. This means that for smaller ΔE_f, the main and second resistance peaks cannot be *observed*.

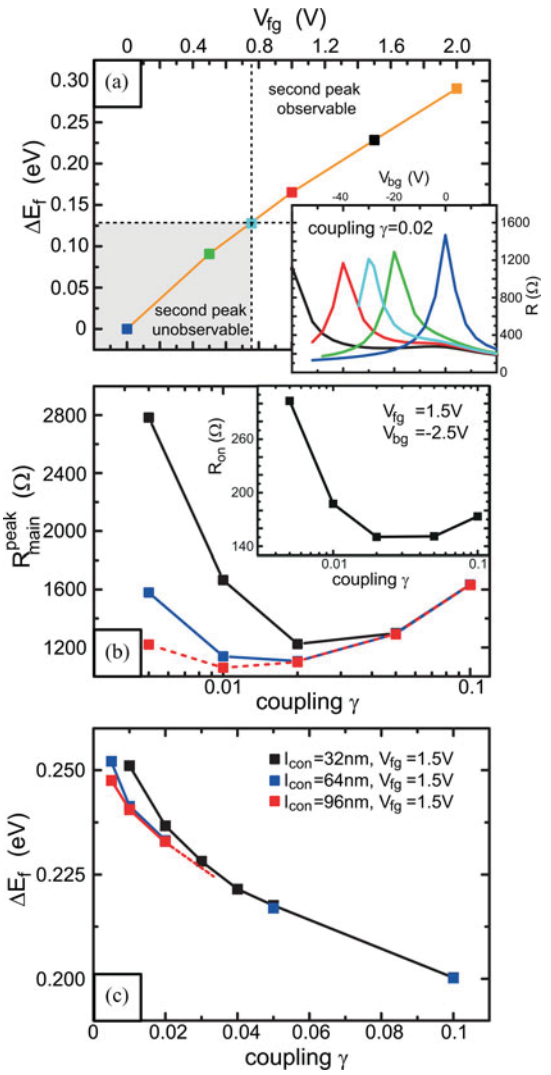

Fig. 6. (a) ΔE_f as a function of $V_{\rm fg}$ as extracted from the simulations at a $V_{\rm bg}$ corresponding to the main resistance peak. The inset shows again resistance versus $V_{\rm bg}$ characteristics that allow determining the $V_{\rm fg}$ where the second resistance peak becomes observable. (b) Main resistance peak as a function of γ for the three contact lengths. The inset displays exemplarily the resistance in the on-state of the graphene device as a function of γ. (c) Difference between Fermi level and Dirac point as a function of γ for three different $l_{\rm con}$.

It was discussed previously that in the experiments presented here, $V_{\rm bg} \approx 25$ V is required in order to compensate the metal-induced doping effect [see Fig. 3(b)]. Taking the scaling factor of ~ 40 of the back-gate voltage (introduced above[1]) into account, one finds from Fig. 6(a) at $V_{\rm fg} = 25/40 = 0.625$ V a $\Delta E_f \approx 100$ meV consistent with the unobservability of the second resistance peak in our experiments for $V_{\rm fg} = 0$ and with 80 meV assumed in [12].

It is worth rephrasing the observations made so far: The second resistance peak should be observable for $\Delta E_f \geq 125$ meV if the coupling is not too large. However, in the experiments presented in [12], $\Delta E_f \approx 80$ meV, and hence, an observability of the second resistance peak is actually not expected (note that in [12], the same contact material was used as in our experiments). Furthermore, in [12], the authors assumed a large variation of the metal–graphene distance $t_{\rm vdW}$ yielding a rather weak average coupling with a lifetime broadening of the electronic states of only 5 meV (whereas we assume ~ 50 meV consistent with [7]) that in turn would lead to a pronounced second resistance peak. According to [12], the second peak is smeared out completely due to the large variation of ΔE_f that goes along with a variation of $t_{\rm vdW}$. However, if such a large variation of contact properties actually existed, a second resistance peak would not be observable even for larger ΔE_f as accessible with our dual-gate device structure. The fact that we do observe experimentally the second resistance peak by creating various ΔE_f shows that the metal–graphene contact properties are not determined by a large variation and rather weak coupling but instead can be described by a larger coupling consistent with theoretical predictions of the lifetime broadening in metal–nanotube contacts [7].

The unobservability of the second resistance peak in single-gated GFETs explains in retrospect why only device type B allows studying the metal–graphene coupling: in device A, the contact areas (consisting of region I and the metal–graphene coupling section) are basically single-gated GFETs where the *I–V* characteristics are dominated by the main resistance peak related to region I. As a result, device A shows two resistance peaks (see also [13]); however, neither is related to the metal–graphene coupling, and hence, device A behaves as if region I was contacted with a coupling close to zero.

V. Discussion—Dependence of Contact Properties on the Coupling

In contrast to conventional metal–semiconductor contacts where the Fermi level is pinned, the possibility to influence the metal–graphene contact with a gate leads to a different dependence of the contact properties on the metal–graphene coupling strength. Having confirmed that our model reproduces all relevant experimental features, we have performed simulations of the main peak resistance for different γ and $l_{\rm con}$, respectively. In a recent publication, density functional theory calculations were performed in order to calculate ΔE_f of different metals in contact with graphene. It was found that ΔE_f sensitively depends on the metal–graphene distance $t_{\rm vdW}$ [19]. Increasing $t_{\rm vdW}$ results in a substantially increased ΔE_f due to the metal–graphene chemical interaction [19]. However, in the present analysis, we have neglected this additional term of chemical interaction and have focused on the mere effect of a varying metal–graphene coupling strength. It is important to note, though, that when taking the chemical interaction into account, our findings are qualitatively still valid and will merely be more pronounced.

Fig. 6(b) shows the peak resistance as a function of γ for three different contact lengths $l_{\rm con}$. In the case of small coupling strength, the peak resistance increases if γ is decreased as well as if $l_{\rm con}$ is made shorter. The reason for this is that the coupling strength determines a minimum contact or transfer length $l_{\rm con}^{\rm min}$ needed in order to obtain a low contact resistance, i.e., a transmission efficiency close to 1. An estimate of $l_{\rm con}^{\rm min}$ can be obtained by expressing γ in terms of a mean free

path for scattering. This mean free path represents the length needed for a carrier to be fully transferred from the metal to the graphene and vice versa. Following Venugopal *et al*. [20], we deduce for the mean free path $l_{\mathrm{con}}\min \approx 2a/\gamma$, where a is the lattice spacing of the finite difference grid [see Fig. 4(a)]. For a coupling strength of $\gamma = 0.02$ as was used in the analysis above, a minimum contact length of ≈ 40 nm is required. Consequently, the resistance peak strongly increases particularly in the case $l_{\mathrm{con}} = 32$ nm for $\gamma \leq 0.02$ since $l_{\mathrm{con}}^{\min} > l_{\mathrm{con}}$ in this case. While a high peak resistance is beneficial since it represents the off-state of the device, the same trend with strongly increasing resistance is also obtained in the on-state of the device as displayed in the inset of Fig. 6(b). This behavior is expected and would also be observed in contacts between a metal and a conventional semiconductor [21], [22]. Interestingly, the peak resistance and the on-state resistance also increase in the case of stronger coupling (i.e., $\gamma > 0.02$). This effect is unexpected in conventional metal–semiconductor contacts. The reason for this peculiar behavior becomes apparent when inspecting Fig. 6(c). Here, ΔE_f is plotted as a function of coupling for the three contact lengths. As γ is increased, the DOS within the contact regions increases [see Fig. 4(c)], and hence, a larger density of carriers is present in the graphene underneath the metallic electrodes. Hence, a gating action (due to a work-function difference or due to a gate voltage) is screened yielding a smaller ΔE_f. In turn, this leads to a smaller shift between the main and second resistance peak eventually yielding an increase of the resistance (see Fig. 2). This observation is still valid when the effect of the chemical metal–graphene interaction is taken into account. In this case, decreasing the metal–graphene separation t_{vdW} significantly decreases ΔE_f resulting again in a resistance increase. Therefore, the metal–graphene coupling strength should be rather small to create low resistive contacts since this enables a larger metal-induced doping effect. However, at the same time, the coupling should not be too small since this makes rather long contact electrodes necessary.

VI. Conclusion

We have studied the impact of the metal–graphene coupling on the performance of GFETs with experiments and simulations. A dual-gate device structure allowed separating the Dirac points within the channel and the contacts by applying an appropriate front- and back-gate voltages. We were able to observe two peaks in the resistance versus back-gate voltage characteristics where the main peak belongs to an alignment of the Fermi level with the Dirac point in the channel and the second, much weaker peak, corresponds to an alignment of the Fermi level with the Dirac point in the contacts. Comparing the experimental data with simulations, we found that the metal–graphene coupling strength is moderate, resulting in a modification of the graphene DOS underneath the contacts small enough so that Fermi level pinning does not occur due to a lack of screening of the gate field. On the other hand, the coupling is strong enough yielding a substantial broadening of the second resistance peak. In addition, the metal-induced doping effect, i.e., the shift of the Fermi level with respect to the Dirac point is less than 100 meV, making the second resistance peak in single-gate GFETs unobservable. Our simulations suggest that a medium coupling strength is most favorable since it provides the best tradeoff between minimum contact length and maximum metal-induced doping effect.

References

[1] K. S. Novoselov, A. K. Geim, S. V. Morozov, D. Jiang, M. I. Katsnelson, I. V. Grigorieva, S. V. Dubonos, and A. A. Firsov, "Two-dimensional gas of massless Dirac fermions in graphene," *Nature*, vol. 438, pp. 197–200, 2005.

[2] A. H. C. Neto, F. Guinea, N. M. R. Peres, K. S. Novoselov, and A. K. Geim, "The electronic properties of graphene," *Rev. Modern Phys*., vol. 81, pp. 109–162, 2009.

[3] K. S. Novoselov, A. K. Geim, S. V. Morozov, D. Jiang, Y. Zhang, S. V. Dubonos, I. V. Grigorieva, and A. A. Firsov, "Electric field effect in atomically thin carbon films," *Science*, vol. 306, pp. 666–669, 2004.

[4] I. Meric, N. Baklitskaya, P. Kim, and K. L. Shepard, "RF performance of top-gated graphene field-effect transistors," in *Proc. IEEE Int. Electron Dev. Meet*., 2008, pp. 1–4.

[5] Y.-M. Lin, C. Dimitrakopoulos, K. A. Jenkins, D. B. Farmer, H. Y. Chiu, A. Grill, and P. Avouris, "100-GHz transistor from wafer-scale epitaxial graphene," *Science*, vol. 327, p. 662, 2010.

[6] Z. Chen, J. Appenzeller, J. Knoch, Y.-M. Lin, and P. Avouris, "The role of metal-nanotube contact in the performance of carbon nanotube field-effect transistors," *Nano Lett*., vol. 5, no. 7, pp. 1497–1502, 2005.

[7] N. Nemec, D. Tomanek, and G. Cuniberti, "Contact dependence of carrier injection in carbon nanotubes: An ab initio study," *Phys. Rev. Lett*., vol. 96, pp. 076802-1–076802-4, 2006.

[8] J. Knoch and J. Appenzeller, "Tunneling phenomena in carbon nanotube field-effect transistors," *Phys. Stat. Solidi A*, vol. 205, pp. 679–694, 2008.

[9] H. Ghoneim, J. Knoch, H. Riel, D. Webb, M. T. Bjoerk, S. Karg, E. Loertscher, H. Schnit, and W. Riess, "Suppression of ambipolar behavior in metallic source/drain metal-oxide-semiconductor field-effect transistors," *Appl. Phys. Lett*., vol. 95, pp. 213504-1–213504-3, 2009.

[10] D. Connelly, C. Faulkner, P. A. Clifton, and D. E. Grupp, "Fermi level depinning for low-barrier Schottky source/drain transistors," *Appl. Phys. Lett*., vol. 88, pp. 012105-1–012105-3, 2006.

[11] Z. Chen and J. Appenzeller, "Gate modulation of graphene contacts—On the scaling of graphene FETs," in *Proc. Symp. VLSI Technol*., 2009, pp. 128–129.

[12] F. Xia, V. Perebeinos, Y.-M. Lin, Y. Wu, and P. Avouris, "The origins and limits of metal-graphene junctions resistance," *Nature Nanotech*., vol. 6, pp. 179–184, 2011.

[13] B. Huard, J.A. Sulpizio, N. Stander, K. Todd, B. Yang, and D. Goldhabe-Gordon, "Transport measurements across a tunable potential barrier in graphene," *Phys. Rev. Lett*., vol. 98, pp. 236803-1–236803-4, 2007.

[14] S. Datta, *Electronic Transport in Mesoscopic Systems*. Cambridge, U.K.: Cambridge Univ. Press, 1998.

[15] R.-H. Yan, A. Ourmazd, and K. Lee, "Scaling the Si MOSFET: From bulk to SOI to bulk," *IEEE Trans. Electron Dev*., vol. 39, pp. 1704–1710, 1992.

[16] R. Venugopal, Z. Ren, S. Datta, M. S. Lundstrom, and D. Jovanovic, "Simulating quantum transport in nanoscale transistors: Real versus mode-space approaches," *Appl. Phys. Lett*., vol. 92, pp. 3730–3739, 2002.

[17] K. P. Clark, W. P. Kirk, and A. C. Seabaugh, "Nonparabolicity effects in the bipolar quantum-well resonant-tunneling transistor," *Phys. Rev. B*, vol. 55, pp. 7068–7072, 1997.

[18] H. Flietner, "E(k) relation for 2-band scheme of semiconductors and application to metal-semiconductor contact," *Phys. Stat. Solidi*, vol. 54, pp. 201–208, 1972.

[19] G. Giovannetti, P. A. Khomyakov, G. Brocks, V. M. Karpan, J. van den Brnk, and P. J. Kelly, "Doping graphene with metal contacts," *Phys. Rev. Lett*., vol. 101, pp. 026803-1–026803-4, 2008.

[20] R. Venugopal, M. Paulsson, S. Goasguen, S. Datta, and M.S. Lundstrom, "A simple transport in nanoscale transistor," *J. Appl. Phys*., vol. 93, pp. 5613–5625, 2003.

[21] W. M. Loh, S. E. Swirhun, T. A. Schreyer, R. M. Swason, and K. C. Saraswat, "Modeling and measurement of contact resistance," *IEEE Trans. Electron Dev*., vol. 34, no. 3, pp. 512–524, Mar. 1987.

[22] L. K Mak, C. M. Rogers, and D. C. Northrop, "Specific contact resistance measurements on semiconductors," *J. Phys. E: Sci. Instrum*., vol. 22, pp. 317–321, 1989.

Joachim Knoch received the Diploma and Ph.D. degrees in physics from RWTH Aachen University, Germany, in 1998 and 2001, respectively.

After postdoctoral research on InP HEMTs at the Microsystems Technology Laboratory, Massachusetts Institute of Technology, he joined the Research Center Juelich in Germany as a Research, where he investigated electronic transport in alternative field-effect transistors such as carbon nanotube FETs, ultrathin-body Schottky-barrier devices and band-to-band tunnel FETs. In December 2006, he accepted a position as permanent research staff member at IBM Zurich Research Laboratory, Switzerland, working on nanowire transistors with an emphasis on tunnel FETs. In September 2008, he was appointed associate professor of electrical engineering at TU Dortmund University, Germany and since May 2011, he has been full Professor and Head of the Institute of Semiconductor Electronics at RWTH Aachen University.

Zhihong Chen received the B.S. degree in physics from Fudan University, Shanghai, China, in 1998, and the Ph.D. degree in physics from the University of Florida, in 2003.

After two years of postdoctoral research at IBM T.J. Watson research center, she became a research staff member in the Physical Science Department. Her research focused on the physical properties of carbon based materials, which involved design and fabrication of high performance devices and circuits. In 2008, she was appointed as the manager of the Carbon Technology Group at IBM, where she was in charge of evaluating the potential of carbon materials and the development of novel carbon based technologies for commercial applications. Since Oct. 2010, she joined the School of Electrical and Computer Engineering at Purdue University, as an associate professor.

Joerg Appenzeller received the M.S. and Ph.D. degrees in physics from the Technical University of Aachen, Germany, in 1991 and 1995. His Ph.D. dissertation investigated quantum transport phenomena in low dimensional systems based on III/V heterostructures.

He worked for one year as a Research Scientist in the Research Center in Juelich, Germany before he became an Assistant Professor with the Technical University of Aachen in 1996. During his professorship he explored mesoscopic electron transport in different materials including carbon nanotubes and superconductor-semiconductor-hybride devices. From 1998 to 1999, he was with the Massachusetts Institute of Technology, Cambridge, as a Visiting Scientist, exploring the ultimate scaling limits of silicon MOSFET devices. From 2001 until 2007, he had been with the IBM T.J. Watson Research Center, Yorktown, NY, as a Research Staff Member mainly involved in the investigation of the potential of carbon nanotubes and silicon nanowires for a future nanoelectronics. Since 2007, he has been a Professor of Electrical and Computer Engineering at Purdue University and Scientific Director of Nanoelectronics in the Birck Nanotechnology Center. His current interests include novel devices based on low-dimensional nano-materials as nanowires, nanotubes and graphene.